Optical properties of Rydberg excitons in Cu_2O-based superlattices

David Ziemkiewicz,* Gerard Czajkowski, and Sylwia Zielińska-Raczyńska
Institute of Mathematics and Physics, UTP University of Science and Technology, Alica Prof. S. Kaliskiego 7, 85-789 Bydgoszcz, Poland

(Received 21 August 2023; revised 7 November 2023; accepted 7 February 2024; published 21 February 2024)

Combining the microscopic calculation of superlattice minibands and macroscopic real density matrix approach, one can obtain electric susceptibilities of the superlattice system irradiated by an electromagnetic wave. It is shown how to calculate the dispersion relation, excitonic resonance positions, and susceptibility of a Cu_2O/MgO-based superlattice (SL), when Rydberg exciton polaritons appear, including the effect of the coherence between the electron-hole pair and the electromagnetic field and the polaritonic effect. Using the Kronig-Penney model for computing miniband SL parameters, analytical expressions for optical functions are obtained and numerical calculations for a Cu_2O/MgO SL are performed.

DOI: 10.1103/PhysRevB.109.085309

I. INTRODUCTION

Excitons, Coulomb-bound pairs of a one-conduction-band electron and a one-valence-band hole, form an electrical neutral quasiparticle, transferring the energy without transporting the net electric charge [1]. Those quasiparticles are complex many-body states embedded in the background of a crystal lattice, which interact via scattering and screening. Therefore, the problem of a manipulation of exciton states through an application of artificial periodic potentials systems has attracted a lot of attention; some implementations include colloidal semiconductor nanocrystals [2], microrod arrays [3], and micropillars [4]. As pointed out in Ref. [5], so-called structured excitons can be used as a means of transporting information and energy in quantum information processing. From this point of view, controlling these excitons in a superlattice [6] can be a very interesting problem. Such a system causes a large shift of exciton energy states and thus influences optical and electronic properties. In principle, a superlattice (SL) containing a Rydberg exciton is a solid-state analog of a Rydberg atom trapped in an optical lattice and can be a promising tool in quantum computing [7–9]. A superlattice can also be used as a medium for exciton-exciton interaction experiments [5]. The relative simplicity and ease of fabrication of a superlattice is an argument for potential application of this nanostructure in quantum information processing. Moreover, in the case of the Cu_2O/MgO system proposed here, when low principal number excitons are used, room-temperature operation is feasible [10].

A superlattice is a periodic structure of layers made of two (or more) semiconductor or insulator materials with different band gaps, where each quantum well imposes new selection rules that affect the conditions for charges to flow through the structure. The two different semiconductor materials are alternately deposited on each other to form a periodic structure in the growth direction. Typically, the width of the layers is of an order of magnitude larger than the lattice constant and is limited by the growth of the structure. Due to the small width of individual layers compared to the illuminating light wavelength, they merge together to form a homogeneous system, which behaves like a bulk crystal. Important requirements of producing a superlattice are a small lattice mismatch and different band-gap energies between the two material components of the structure.

Recently, Yang *et al.* [6] produced a SL based on a cuprite, where the wells consist of a narrow-band-gap semiconductor Cu_2O and the barriers are made of a wide-band-gap insulator MgO. The lattice constants of both of these substances are quite similar with a small mismatch between the constituent layers (with the difference 1.35%), while Cu_2O is a narrow-band-gap semiconductor with $E_g \sim 2.2$ eV and MgO is a wide-band-gap compound with $E_g \sim 8$ eV [6], which satisfy the basic requirements for a good SL structure.

In this paper, we consider a structure of similar dimensions, e.g., the total thickness of the order of 100 nm and individual layer thickness of the order of a few nm. We intend to describe the optical properties of this SL: the optically active layers of cuprous oxide Cu_2O and buffer layer of magnesium oxide MgO. Further, we will discuss the behavior of Rydberg excitons located in the system of quantum wells, which create a system of periodic potentials. Since the first observation of Rydberg excitons (REs) in Cu_2O in 2014 [11], they have become the subject of intensive study. These highly excited states in Cu_2O were observed up to a large principal quantum number $n = 30$ [12]. Due to the unusual properties of REs, such as huge sizes scaling as n^2, long lifetimes reaching nanoseconds, and strong exciton-exciton interactions controlled by so-called Rydberg blockade, REs could have many promising applications as single-photon emitters, single photon transistors, and as active medium of masers [13]. Initial studies on Rydberg excitons were focused at the optical properties of REs in high-quality natural crystals (bulk crystals); see Refs. [14,15] for recent studies. Also, some groups concentrated on fabrication techniques of Cu_2O nanostructures

*david.ziemkiewicz@utp.edu.pl

[16–18]. Recently, the main interest of research has shifted from REs in bulk crystals to excitons in low-dimensional systems [19–21]. The first experimental verification of an oscillator strength change caused by the quantum confinement of REs in a low-dimensional quantum system [22] was an important step forward to exploit them in quantum applications. Therefore, it seems natural to examine the optical properties of REs in the specific type of a nanosystem, which consists of quantum wells forming a lattice of periodic potentials confining REs. The unique property of periodic potential systems represents a possibility to change the effective masses of particles inside such structures. Regarding an exciton in a SL, the electron and the hole effective masses are modified, which results in an adjustment of an optical susceptibility. For a given SL structure geometry, one is able to predict the shift of excitonic resonances positions compared to the bulk case. The last, but not least, argument for choosing this subject is the fact that the optical lattices with neutral atoms have been successfully applied in quantum information devices. In analogy, we imply that due to the inherent, repeating pattern of the SL and long-coherence times of Rydberg excitons, their huge polarizability and dipole moments, which allow them to strongly interact with each other over a long distance, arranged in such systems, they might also be viable candidates for quantum computing.

Band-edge optical properties of superlattices can be discussed by modeling the superlattice as an effective anisotropic medium in which the quasifree carriers propagate and interact. In the low barriers limit, the electron and hole motion in the confinement direction is determined by the superlattice potential and is replaced by an effective-mass motion, with the appropriate effective masses obtained from the miniband dispersion relations [23,24].

Since excitons in the majority of semiconductors are of the Wannier type, the transition dipole has a spatial extension, characterizing the interaction of radiation with electrons and holes located at different sites. This results in a coherence between the electron-hole pair and the radiation field. In analogy to bulk semiconductor excitons, SL excitons induced by an electromagnetic wave propagating through the SL will give rise to "SL polaritons."

As in the bulk crystals, polaritons are mixed modes of the electromagnetic field and discrete excitations of the SL $E_n(\mathbf{k}_{\mathrm{ex}})$ (excitons). Below the gap, one can imagine a polariton as a photon surrounded by a cloud of virtual electron-hole pairs (excitons).

All of the above-mentioned components (Wannier excitons, effective mass approximation, exciton polaritons with coherence) justify the use of the real density matrix approach (RDMA) to describe the optical properties of superlattices. The method has already been used to describe excitons and polaritons in a III-V [25] and II-VI SL [26] and was successful in the description of REs' optical properties of Cu_2O bulk crystals [27], and nanostructures (quantum wells, dots, and wires) [28].

Below we present in detail a procedure of the calculation, which starts with the Kronig-Penney model to obtain SL miniband parameters, i.e., anisotropic effective masses and band gaps. To derive the dispersion relation and resonance positions in a SL, the RDMA with these parameters is used. This method has a general character and allows one to get an analytical formula for a system susceptibility. It takes into account both the Coulomb interaction between an electron and a hole and a coherence between an electron-hole pair and a radiation field. The particular calculations will be done for Cu_2O/MgO SL, for which the SL dielectric tensor and the optical functions in the analytical form will be calculated.

The paper is organized as follows. In Sec. II, we present the basic equations of the Kronig-Penney model adapted to the cases of superlattices. Section III shows the scheme for calculating the SL optical functions in the case in which the total thickness of the SL is much greater than the excitonic Bohr radius. In Sec. IV, results obtained for the Cu_2O/MgO superlattice are discussed, and conclusions are presented in Sec V.

II. KRONIG-PENNEY MODEL FOR SUPERLATTICES

In this section, we recall the basic equations which describe the electronic states (conduction and valence bands) of a superlattice. Considering the Kronig-Penney model, we assume the confinement potential in the z direction (structure growth direction), which for conduction electrons corresponds to $V(z) = 0$ if z corresponds to area inside the well (well thickness L_W, effective mass m_W), and $V(z) = V_0$ if z corresponds to the barrier area (thickness L_B, effective mass m_B), where V_B is the conduction-band offset. The equation for the values of the Bloch vector K, and thus the miniband dispersion [23–29], takes the Kronig-Penney form,

$$\cos KL = \cos k_1 L_W \cosh \kappa_2 L_B - \frac{k_1^2 - \kappa_2^2}{2k_1\kappa_2} \sin k_1 L_W \sinh \kappa_2 L_B, \tag{1}$$

where k_1 and κ_2 are the wave vectors in the well and in the barrier, respectively. The subscripts W and B in Eqs. (1) denote the wells or barriers, and $L = L_W + L_B$ is the SL period. The wave vectors in the well and barrier are

$$k_1 = \sqrt{\frac{2m_W E}{\hbar^2}}, \qquad \kappa_2 = \sqrt{\frac{2m_B(V-E)}{\hbar^2}}. \tag{2}$$

The above equations can be solved for electrons and holes separately, obtaining the relation $E(K)$, where E is the electron/hole energy, m_W and m_B are effective masses in Cu_2O and MgO, and V is the potential barrier between MgO and Cu_2O. Specifically, due to the difference of band-gap energies (see Table I), we have $V_0 = 4.99$ eV. From this, we obtain the electron and hole confinement potentials $V_{0e,h}$,

$$V_0 = E_g(\mathrm{MgO}) - E_g(\mathrm{Cu_20}), \quad V_0 = V_{0e} + V_{0h}, \quad V_{0e} = 0.4 \times V_0, \quad V_{0h} = 0.6 \times V_0. \tag{3}$$

This results in two barrier values, $V_{0e} = 2$ eV and $V_{0h} = 3$ eV, for electrons and holes, respectively. The division of V_0 into electron and hole potential barriers follows from the relative

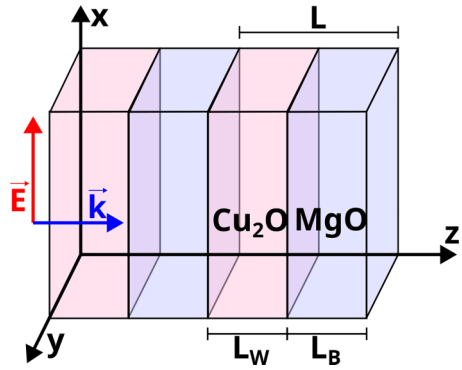

FIG. 1. Schematic representation of the system.

Fermi energy level of Cu_2O [30] and MgO [31] and is similar to the case of the Cu_2O/ZnO heterojunction [32].

One of the important parameters of the SL structure that makes it different from bulk material are the effective masses of a hole and an electron in the z direction, which are determined from the relation

$$\frac{1}{m_z} = \frac{1}{\hbar^2}\frac{d^2E}{dK^2}\bigg|_{K=0}, \tag{4}$$

which, again, can be obtained separately for electrons and holes, from the respective $E(K)$ relations. Note that the dispersive relation of bulk materials is taken into account with effective masses m_W, m_B, and the $E(K)$ relation only describes the dominating superlattice contribution.

III. OPTICAL PROPERTIES

We consider a superlattice which consists of a large number of narrow potential wells of a thickness L_W separated by narrow potential barriers characterized by a thickness L_B, where tunneling effects are allowed. A total thickness of a single well-barrier pair is L. The system is presented in Fig. 1. It is irradiated by a normally incident electromagnetic wave, linearly polarized in the x direction,

$$E_i(z,t) = E_{i0}\exp(ik_0 z - i\omega t), \quad k_0 = \frac{\omega}{c}. \tag{5}$$

We assume that $L < 4$ nm and consider barrier width of less than 2 nm, which is significantly smaller than the diameter of even the lowest $2P$ exciton ($d \sim 8$ nm) in Cu_2O. Therefore, the tunneling through the barrier is allowed despite the barrier height. The individual quantum wells (QWs) merge together into a homogeneous system, which behaves like a bulk crystal; the total number of layers is of the order of 10–100 and the exact number is not relevant to the calculations.

The linear optical response of the system (here we consider the lowest electron and hole miniband) to the electromagnetic wave originates from a given pair of minibands and is described by two equations: the so-called constitutive equation (material equation) and the Maxwell's propagation equation. The constitutive equation has the form

$$-i\hbar\partial_t Y - i\Gamma Y + H_{eh}Y = \mathbf{M}(\mathbf{r})\mathbf{E}(\mathbf{R}), \tag{6}$$

where $Y(\mathbf{R},\mathbf{r},t)$ is the excitonic transition coherent amplitude, Γ is a dissipation coefficient, $\mathbf{M}$ is the transition dipole density, $\mathbf{R}$ is the excitonic center-of-mass coordinate, and $\mathbf{r}$ the relative electron-hole coordinate. The operator H_{eh} is the effective mass Hamiltonian of the superlattice,

$$H_{eh} = E_g + \frac{P_Z^2}{2M_z} + \frac{\mathbf{P}_\parallel^2}{2M_\parallel} + \frac{p_z^2}{2\mu_z} + \frac{\mathbf{p}_\parallel^2}{2\mu_\parallel} + V_{eh}, \tag{7}$$

with V_{eh} being the electron-hole Coulomb interaction. We have separated the center-of-mass coordinate $\mathbf{R}_\parallel$ and the related momentum $\mathbf{P}_\parallel$ from the relative coordinate ρ on the plane (xy) and the related momentum $\mathbf{p}_\parallel$. In the above formulas, the reduced mass in the z direction is given by

$$\frac{1}{\mu_z} = \frac{1}{m_{ez}} + \frac{1}{m_{hz}}, \tag{8}$$

where the electron and the hole effective masses in the z direction follow from the miniband dispersion relations (1), i.e., one for electrons and one for holes, respectively. The system is not confined in the xy directions and so the in-plane effective masses $m_\parallel$ in the well material are assumed to be the same as in the bulk medium. M_z and $M_\parallel$ are the total excitonic masses in the growth direction and parallel to the layers, respectively. We use the same form for the transition dipole density as for bulk semiconductor [27],

$$\begin{aligned}\mathbf{M}(\mathbf{r}) &= \mathbf{e}_r M_{10}\frac{r+r_0}{2r^2r_0^2}e^{-r/r_0} = \mathbf{e}_r M(r)\\ &= \mathbf{i}M_{10}\frac{r+r_0}{4ir^2r_0^2}\sqrt{\frac{8\pi}{3}}(Y_{1,-1}-Y_{1,1})e^{-r/r_0}\\ &+ \mathbf{j}M_{10}\frac{r+r_0}{4r^2r_0^2}\sqrt{\frac{8\pi}{3}}(Y_{1,-1}+Y_{1,1})\,e^{-r/r_0}\\ &+ \mathbf{k}M_{10}\frac{r+r_0}{2r^2r_0^2}\sqrt{\frac{4\pi}{3}}Y_{10}e^{-r/r_0},\end{aligned} \tag{9}$$

where r_0 is the so-called coherence radius,

$$r_0^{-1} = \sqrt{\frac{2\mu}{\hbar^2}E_g}. \tag{10}$$

$Y_{\ell m}$ are spherical harmonics, which are complex-valued functions of the spherical coordinates θ, ϕ. Specifically, we use the definition [33]

$$Y_{\ell,m}(\theta,\phi) = \sqrt{\frac{2\ell+1}{4\pi}\frac{(\ell-m)!}{(\ell+m)!}}\,P_\ell^m(\cos\theta)e^{im\phi}, \tag{11}$$

where $P_{\ell,m}$ are the associated Legendre functions,

$$P_\ell^m(x) = \frac{(-1)^m}{2^\ell\,\ell!}(1-x^2)^{m/2}\frac{d^{\ell+m}}{dx^{\ell+m}}(1-x^2)^\ell. \tag{12}$$

Thorough the manuscript, indices n, l, m are main, angular momentum, and magnetic quantum numbers, respectively.

The above expression gives the coherence radius in terms of effective band parameters E_g (the bulk gap energy) and μ (the electron-hole reduced effective mass; the bulk effective masses of the electron and the hole are assumed to be isotropic). M_{10} is the integrated dipole strength. In order to present the form of the susceptibility with Rydberg excitons adapted for a case of a superlattice, we recall the procedure

similar to that presented in [27]. The steps of the calculation scheme are the following:

(1) The excitonic amplitude Y is determined from Eq. (6) with the Hamiltonian (7).

(2) The coherent amplitude Y enables one to calculate the SL polarization, which is given by the formula [27]

$$\mathbf{P}(\mathbf{R}) = 2\int d^3 r \mathbf{M}(\mathbf{r}) Y(\mathbf{R}, r). \tag{13}$$

(3) The polarization $\mathbf{P}$ is then inserted into the Maxwell propagation equation,

$$c^2 \nabla_R^2 \mathbf{E} - \underline{\underline{\epsilon}}_b \ddot{\mathbf{E}}(\mathbf{R}) = \frac{1}{\epsilon_0}\ddot{\mathbf{P}}(\mathbf{R}), \tag{14}$$

with the use of the bulk dielectric tensor $\underline{\underline{\epsilon}}_b$ and the vacuum dielectric constant ϵ_0.

In analogy to bulk crystals, the description of the SL exciton polaritons is based on the separation of the relative electron-hole motion with well-defined quantum levels from the center-of-mass motion which interacts with the radiation field and produces the mixed modes (polaritons). We assume that the center-of-mass motion is described by the term $\exp(\mathrm{i}\mathbf{k}\,\mathbf{R})$ with the wave vector $\mathbf{k}$. Additionally, we use the electromagnetic wave that has a harmonic time dependence $\propto \exp(-\mathrm{i}\omega t)$. These simplifications allow us to calculate the dielectric susceptibility. Because in Cu_2O the conduction band and the valence band are of the same parity, the dipole moment between them vanishes; the $n > 1$ lines correspond to excitons with the angular momentum $l = 1$ and therefore the absorption process is dipole allowed. Equation (6) will be solved by expanding the coherent amplitude Y in terms of eigenfunctions of the Hamiltonian H_{eh},

$$Y = \sum_{n\ell m} c_{n\ell m} R_{n\ell m}(r) Y_{\ell m}(\theta, \phi). \tag{15}$$

The radial functions $R_{n\ell m}$ are given in the form [33]

$$\begin{aligned} R_{n\ell m}(r) = {} & \left(\frac{2\eta_{\ell m}}{na^*}\right)^{3/2} \frac{1}{(2\ell+1)!}\sqrt{\frac{(n+\ell)!}{2n(n-\ell-1)!}} \\ & \times \left(\frac{2\eta_{\ell m} r}{na^*}\right)^{\ell} e^{-\eta_{\ell m} r/na^*} M \\ & \times \left(-n+\ell+1, 2\ell+2, \frac{2\eta_{\ell m} r}{na^*}\right). \end{aligned} \tag{16}$$

The coefficient η_{lm} depends on an effective masses ratio α, which for the SL is different from that of the bulk and therefore is crucial for eigenvalues $E_{n\ell m}$,

$$\eta_{\ell m} = \int d\Omega \frac{|Y_{\ell m}|^2}{\sqrt{\sin^2\theta + \alpha\cos^2\theta}}, \tag{17}$$

$$\begin{aligned} E_{n\ell m} &= -\frac{\eta_{\ell m}^2(\alpha) R^*}{n^2}, \quad n = 1, 2, \ldots, \\ &\ell = 0, 1, 2, \ldots, n-1, \quad m = 0, 1, 2, \ldots, \ell, \\ \alpha &= \frac{\mu_\parallel}{\mu_z}. \end{aligned} \tag{18}$$

In Eq. (16) above, a^* is the exciton Bohr radius and $M(a, b, z)$ is the Kummer function (confluent hypergeometric function) in the notation of Ref. [34]. The anisotropy parameter α, first introduced by Kohn and Luttinger [35], corresponds to the dimensionality of the system [36,37]; specifically, in the so-called fractional dimensionality approach [38], the system dimension $d = 2 + \sqrt{\alpha}$, so that it is two dimensional in the limit of $\alpha \to 0$ and three dimensional for $\alpha = 1$.

R^* is the effective excitonic Rydberg energy defined as

$$R^* = \frac{\mu_\parallel e^4}{2(4\pi\epsilon_0\sqrt{\epsilon_\parallel\epsilon_z})^2\hbar^2}. \tag{19}$$

Modified by the periodic potential of the SL effective masses, one can calculate the anisotropy factor α and the corresponding eigenvalues $E_{n\ell m}$ from Eq. (18). In the considered case of P excitons, we use the quantities

$$\begin{aligned} \eta_{00}(\alpha) &= \frac{\arcsin\sqrt{1-\alpha}}{\sqrt{1-\alpha}}, \\ \eta_{10}(\alpha) &= \frac{3}{2(1-\alpha)}(\eta_{00} - \sqrt{\alpha}), \\ \eta_{11}(\alpha) &= \frac{3}{2}\left[\eta_{00}(\alpha) - \frac{1}{3}\eta_{10}(\alpha)\right]. \end{aligned} \tag{20}$$

The energies for the electron and hole $E_{0e,h} = E_{e,h}(K = 0)$ determine the SL energy gap,

$$E_g(\mathrm{SL}) = E_g + E_{0e} + E_{0h}, \tag{21}$$

which is shifted by $E_{0e} + E_{0h}$ as compared to the bulk. The eigenenergies $E_{n\ell m}$ affect the positions of the SL excitonic resonances, given by the transverse energies $E_{Tn\ell m}$,

$$E_{Tn\ell m} = E_g(\mathrm{SL}) + E_{n\ell m}, \tag{22}$$

which are, in consequence, also moved due to the modification of effective masses by the influence of the SL periodic potentials' pattern.

Since the superlattice consists of multiple quantum wells, it is justified to assume that the symmetry properties of excitons in the SL are similar to those in quantum wells. The considered system geometry (see Fig. 1) and the electric field polarization (5) allow one to use the x component of the dipole density (9),

$$M_x(r) = M_{10}\frac{r + r_0}{4\mathrm{i}r^2 r_0^2}\sqrt{\frac{8\pi}{3}}(Y_{1,-1} - Y_{1,1})e^{-r/r_0}. \tag{23}$$

With the help of Eqs. (16) and (23), the expansion coefficients $c_{n\ell m}$ are calculated. Then the coherent amplitude Y is used in Eq. (13), which in turn is inserted into the Maxwell equation (14), from which one obtains the dispersion relation for SL polaritons,

$$\frac{c^2k^2}{\omega^2} - \epsilon_b = \epsilon_b \sum_{n=2}^{N} \frac{\Delta_{LT}^{(P)} f_{n11}}{E_{Tn11} - \hbar\omega + (\hbar^2k^2/2M_z) - i\Gamma_n}, \tag{24}$$

with

$$f_{n11} = \frac{32}{3}\frac{(n^2-1)\eta_{11}^5}{n^5}. \tag{25}$$

$\Delta_{LT}^{(P)}$ is the longitudinal-transversal splitting energy, and E_{Tn11} are the energies of excitonic resonances [see Eq. (22)]. The

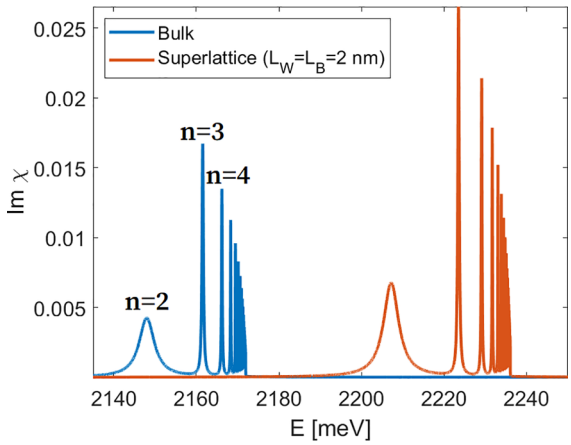

FIG. 2. Comparison of the imaginary part of susceptibility in a bulk Cu_2O and in a Cu_2O/MgO SL, calculated from Eq. (26). The first few excitonic states $n = 2, \ldots, 4$ are marked.

relation [39]

$$|M_{10}|^2 = \frac{4\epsilon_0\epsilon_b a^{*3}\Delta_{LT}^{(P)}}{\pi(r_0/a^*)^2}$$

has been used. In the considered narrow frequency range, one can use $\epsilon_b = \text{const} = 7.5$ [11].

The spatial dispersion, described by (24), makes it possible to have two or more wave modes connected with a given frequency. The term $\hbar^2k^2/2M_z$ in the denominator on the right-hand side of Eq. (24) is responsible for the effect of multiplicity of polariton waves. In the considered case of a Cu_2O/MgO SL, the total exciton mass M_z is much larger than in other semiconductors (both bulk and SL), so it is justified to neglect this term. As pointed out in [40], a relatively small oscillator strength and resulting weak light-exciton coupling in bulk Cu_2O makes it difficult to achieve the strong-coupling regime that is necessary for polaritonic effects to become significant. It is demonstrated in [40] that this problem can be solved by placing the crystal between two Bragg reflectors, forming a cavity; multiple, strong reflections on the Cu_2O/MgO interfaces considered here might provide another way to achieve a strong-coupling regime. In view of the above findings, we obtain the excitonic contribution to the linear optical susceptibility in the form

$$\chi(\omega) = \epsilon_b \sum_{n=2}^{N} \frac{\Delta_{LT}^{(P)} f_{n11}}{E_{Tn11} - \hbar\omega - i\Gamma_n}. \tag{26}$$

In particular, we are interested in the imaginary part of the susceptibility, where absorption maxima corresponding to excitonic states can be observed; we note that in this energy region, MgO is mostly transparent. In our calculations, we do not include nonexcitonic contributions to the absorption of Cu_2O, which provide approximately 25% of the total absorption coefficient in the region of excitonic maxima [11].

IV. RESULTS

The above presented scheme allows for the calculation of all optical SL functions. We have chosen the optical susceptibility since its imaginary part is proportional to the SL absorption. We have computed the susceptibility Cu_2O/MgO SL for a variety of Cu_2O QW and MgO barrier thicknesses. The values of the relevant parameters are given in Table I. The obtained results are illustrated in Figs. 2–9.

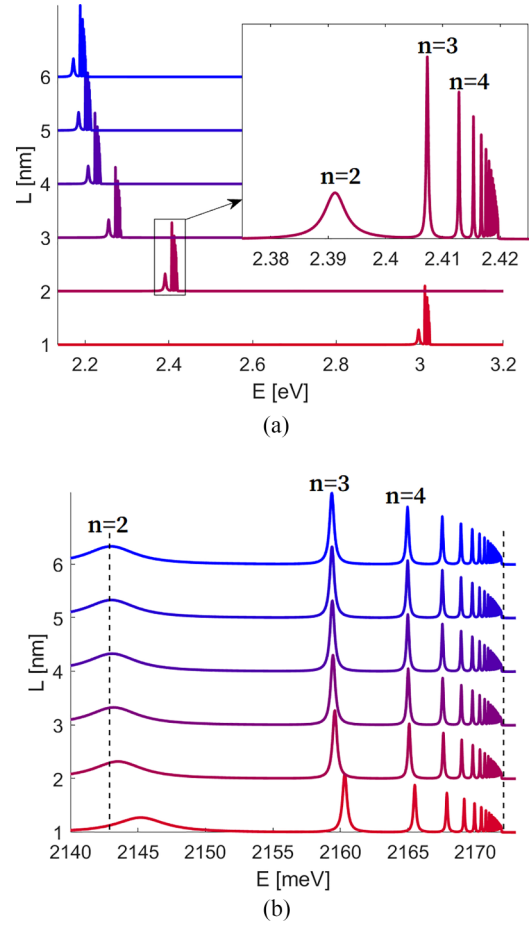

FIG. 3. Imaginary part of the superlattice susceptibility (a) with and (b) without the lowest Cu_2O/MgO SL band energy shift included. Inset: Zoom-in of excitonic spectrum for $L = 2$ nm.

Figure 2 presents the imaginary part of the susceptibility of bulk Cu_2O and a superlattice with $L = 4$ nm ($L_W = L_B = 2$ nm). Even for such a relatively large L (of the order of 10 lattice constants), the energy shifts E_{e0}, E_{h0} are considerably larger than the energy spacing of the excitonic levels. The two key features visible in Fig. 2 are a slight increase of the oscillator strength (proportional to the area under the absorption peak) in the SL, as well as a slight modification of the Rydberg energy, in accordance with Eq. (19).

As the SL period L is decreased, the energy shift increases proportionally to $\sim 1/L$. This is shown in Fig. 3(a). For values $L < 4$ nm, the shift exceeds the total width of the excitonic spectrum, which means that the confinement energy exceeds the Rydberg energy, which is a necessary condition for the strong confinement regime assumed here. It should be stressed that the energy shift of the excitonic spectrum is very considerable, exceeding 1 eV for $L < 1$ nm. By omitting the energy shifts E_{e0}, E_{h0} [Fig. 3(b)], one can see the weaker effects; as L decreases, there is a slight decrease of the Rydberg energy. One can see this by comparing the spectra in Fig. 3(b) with the

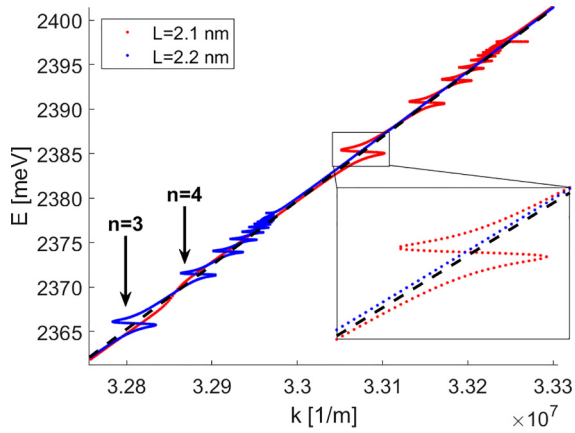

FIG. 4. Polariton dispersion relation of the Cu_2O/MgO superlattice, calculated from Eq. (24), for two values of the SL period L. The dashed line marks the dispersion relation calculated for $\epsilon_b = 7.5$, without excitonic effects. Inset: Zoom-in of a single excitonic resonance.

dashed, vertical lines that mark the $n = 2$ exciton energy and gap energy for $L = 6$ nm, which is close to a bulk. In general, exciton energies and related optical properties of the system approach bulk values in the limit $L \to \infty$. For small values of L, the excitonic spectrum becomes visibly narrower, which is the result of a smaller effective Rydberg energy $\eta^2_{\ell m}(\alpha)R^*$.

For further insight into the properties of the system, one can calculate the dispersion relation from Eq. (24). The results for two values of L ($L_W = L_B = L/2$) are shown in Fig. 4. A similar shape of the function $E(K)$ is present for each excitonic resonance ($n = 3$ is visible in the lower-left corner). Overall, the excitons result in a small, localized disturbance of the bulk dispersion relation (dashed line), which is energy shifted depending on the value of L. Notably, even a small change from $L = 2.1$ to $L = 2.2$ nm results in an energy shift comparable to the width of the entire excitonic spectrum.

To calculate the relevant quantities, such as electron and hole effective masses in the z direction and the anisotropy parameter α, one has to numerically solve Eq. (1). The results obtained for a few selected values of L_W, L_B are presented in Fig. 5. For the smallest well and barrier widths, approximately equal to that of a single atomic layer, only two electron/hole band pairs are visible in the energy range $E < 5$ eV. The lowest band is characterized by a positive effective mass, while the masses in the second band are negative and relatively small ($\partial^2 E/\partial k^2 \ll 0$). An increase of both the well thickness and the barrier width result in a higher density of bands, although the effect of increased L_B is less significant. Notably, the dispersion relation of the lowest band becomes extremely flat, especially for holes ($\partial^2 E/\partial k^2 \to 0$), which results in a very big hole effective mass in the z direction.

Figure 6 depicts the effective electron and hole masses [Eq. (4)] as well as anisotropy parameter α [Eqs. (8) and (18)] as a function of L_W, where $L_W + L_B = 1.4$ nm. One can see that there are some optimal values of $L_W = 0.5$ nm, $L_B = 1.5$ nm, where effective masses reach their maximum value. The anisotropy parameter reaches a minimum value $\alpha \approx 0.25$ for a slightly smaller well width. As mentioned above, the effective mass of the hole can reach a very high value in the considered system, up to $m_z \sim 70\ m_0$, while the

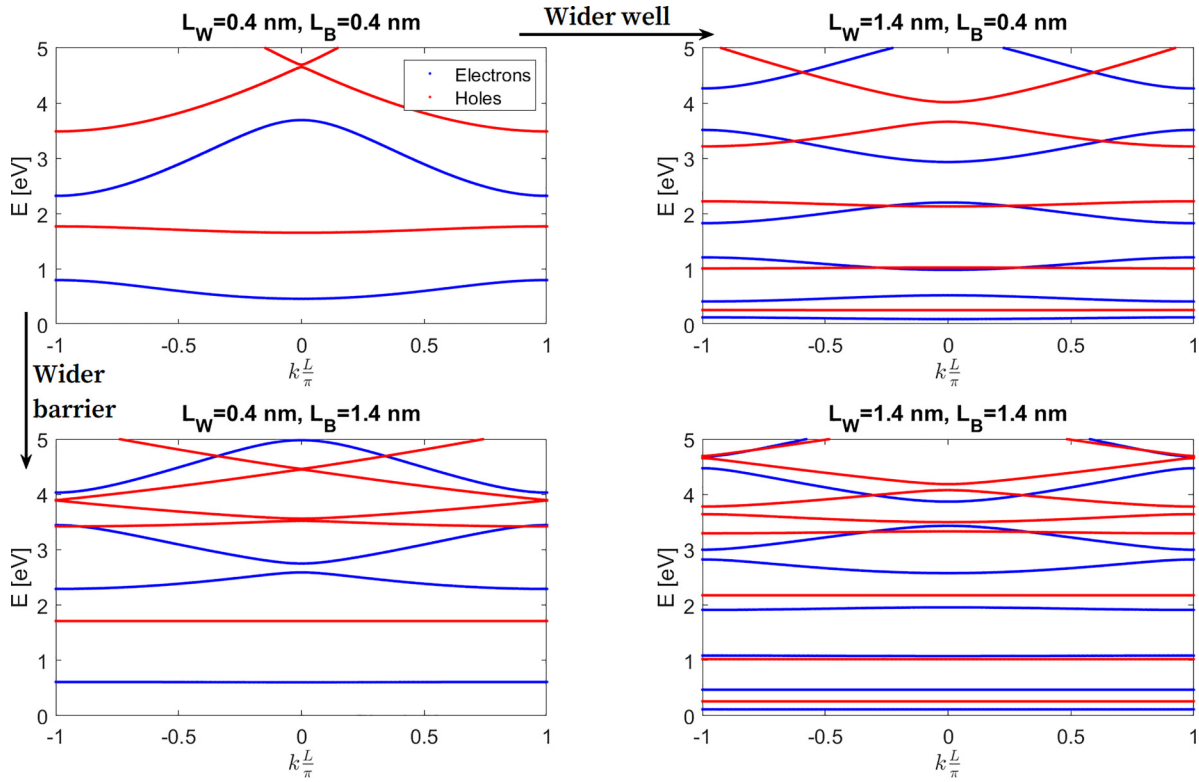

FIG. 5. SL dispersion relations of electrons and holes, calculated from Eq. (1), for various values of well (L_W) and barrier (L_B) widths.

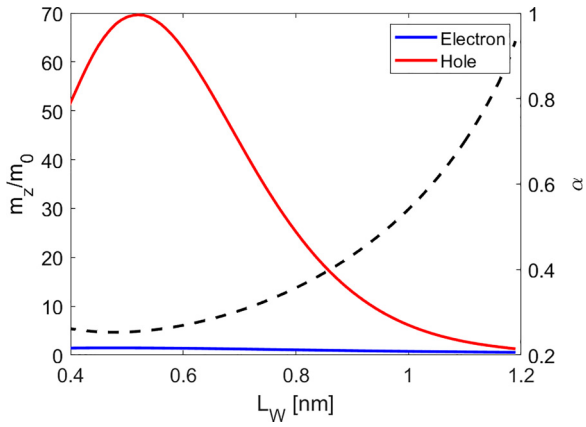

FIG. 6. Electron and hole effective masses [Eq. (4), left axis] and anisotropy parameter α [calculated from Eqs. (8) and (18), right axis] of the Cu_2O/MgO SL, as a function of L_W; $L_W + L_B = 1.4$ nm.

effective electron mass does not exceed 3 m_0, where m_0 is the electron mass in bulk crystal. A significantly increased effective mass in the z direction means that the system approaches a quasi-two-dimensional one, with only two degrees of freedom (x, y) for the exciton motion. This is reflected in a small value of the anisotropy parameter α.

An overview of effective mass values for a range of L_W, L_B is shown in Fig. 7. In the limit of wide barriers, the effective mass of a hole can reach values of up to 10^3 m_0. In practice, this means that the hole cannot tunnel through the potential barrier and the system becomes two dimensional, allowing only for the motion in the xy plane. In such a case, the structure is no longer a superlattice, but a set of separated quantum wells (a multiwell system). The obtained results confirm that the barrier width should not considerably exceed the Bohr radius of the exciton (1.1 nm). It should be stressed that the small barrier width is a necessary condition for the tunnelling to occur, which is needed for the validity of the presented approach. Another effect visible in Fig. 7 is that in the case of a narrow well ($L_W < 1$ nm), the increase of the effective mass is slower due to the fact that the well thickness is smaller than the exciton diameter, so that its wave function enters the barriers, facilitating an easier tunneling through them. One can also see that in the limit of large L_W, the effective mass stops increasing with L_W and is only a function of L_B. Finally,

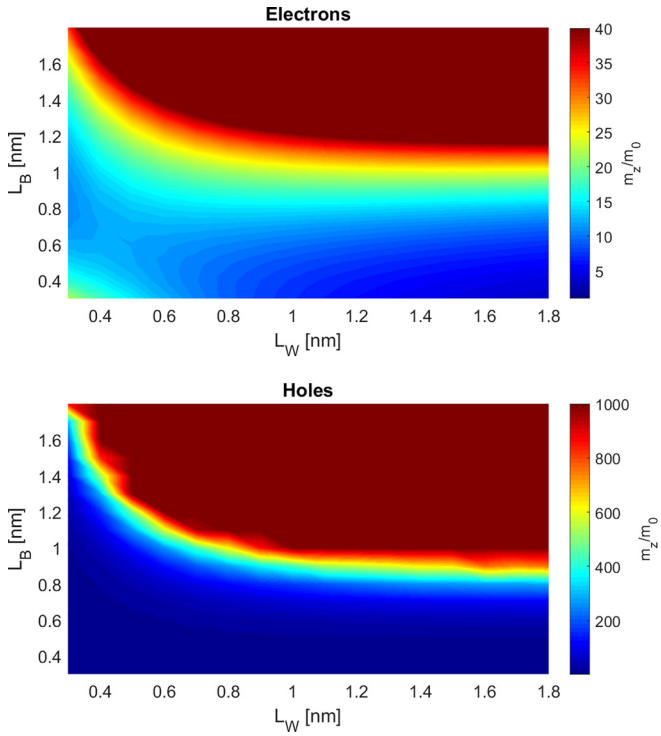

FIG. 7. Electron and hole effective masses in the Cu_2O/MgO SL as a function of L_W and L_B, calculated from Eq. (4).

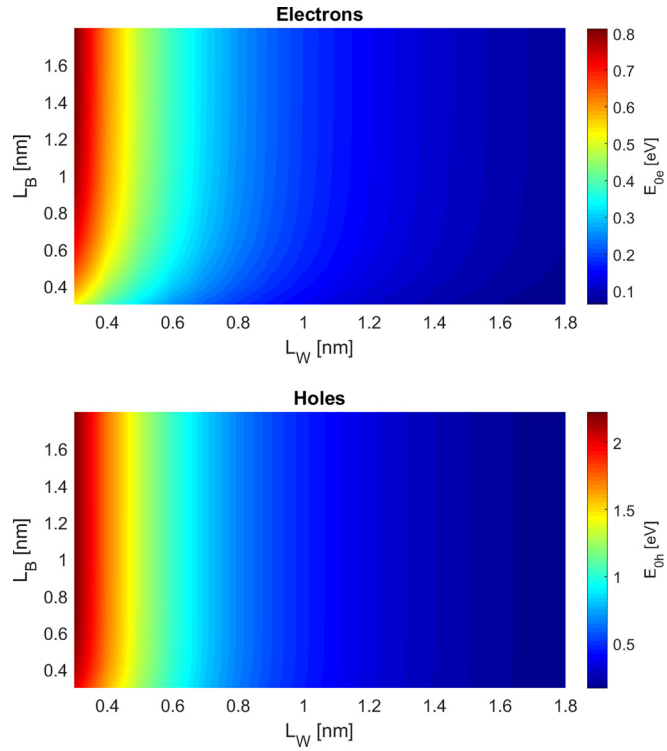

FIG. 8. The energy of the lowest electron and hole band in the Cu_2O/MgO SL, as a function of L_W and L_B, calculated from Eq. (1).

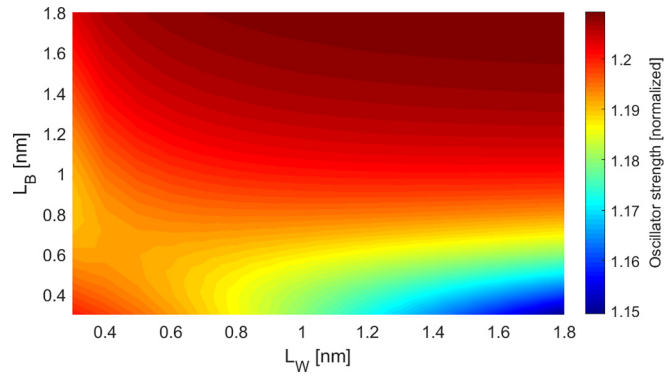

FIG. 9. Exciton oscillator strength in Cu_2O/MgO SL, as a function of L_W and L_B, calculated from Eq. (25), normalized to the bulk value.

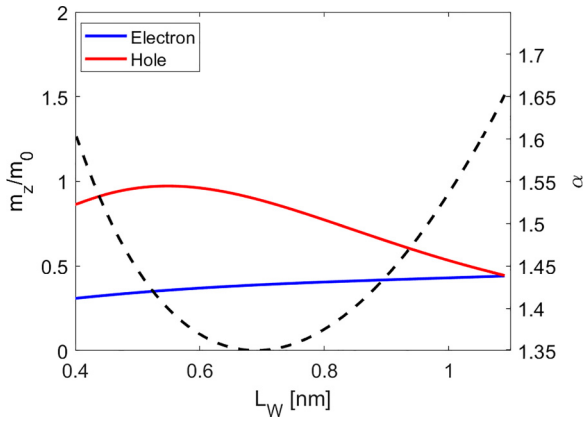

FIG. 10. Electron and hole effective masses [Eq. (4), left axis] and anisotropy parameter α [calculated from Eqs. (8) and (18), right axis] of the Cu_2O/ZnO SL, as a function of L_W; $L_W + L_B = 1.4$ nm.

we note that the bulk effective mass can be obtained from the model in the limits of both $L_W \to \infty$ and $L_B \to 0$.

Figure 8 depicts the lowest polariton band energy as a function of L_W, L_B. One can see that the energy dependence on the well width is much more pronounced, resulting in $E_{0e} \sim 0.8$ eV and $E_{0h} \sim 2.2$ eV for $L_W = 0.4$ nm. This result is analogous to the case of a single quantum well, where the energy of the lowest level strongly depends on the well width.

Finally, in Fig. 9, one can see that the effective oscillator strength of the excitons is slightly enhanced in the SL, in particular when both the barrier and the well thickness are large. This is an expected result—as the effective masses m_{ez} and m_{hz} increase, the reduced mass μ_z [Eq. (8)] also increases and the anisotropy parameter α [Eq. (18)] is decreasing. This, according to Eq. (20), affects the oscillator strength.

A superlattice containing Cu_2O can use various barrier materials; one of the possibilities is ZnO [32]. In contrast to MgO, ZnO is a semiconductor with a relatively narrow band gap, $E_g = 3.4$ eV [41], which results in barrier energies of $E_{0e} = 0.7$ eV and $E_{0h} = 1.88$ eV. The relatively small value of the barrier yields low effective masses in the z direction and a large value of α. The results of the calculations are shown in Fig. 10. The material parameters used in the calculations are given in Table I.

TABLE I. Parameter values for bulk Cu_2O, MgO, and ZnO. Masses in free electron mass m_0, R^* calculated from $(\mu/\epsilon_b^2) \times 13\,600$ meV, $R^*_{e,h} = (m_{e,h}/\mu)R^*$ calculated by the assumption that the masses in the $x-y$ plane remain unaltered, lengths in nm, $a^*_{e,h} = (\mu/m_{e,h})a^*$.

Parameter	Cu_2O (bulk)	MgO (bulk)	ZnO (bulk)	References
E_g	2172.08	7160	3400	[11,41,42]
R^*	87.78		60	[41]
Δ_{LT}	0.0125			[45]
m_{ez}	0.99	0.378	0.24	[41,43,44,46]
$m_{h\parallel}$	0.58	1.575	0.54	[41,43,44,46]
m_{hz}	0.58	1.575	0.54	[41,43,44,46]
$\mu_\parallel$	0.363	0.319	0.17	
μ_z	0.363	0.319	0.17	
M_z	1.56	1.953	0.83	
α	1	1	1	
a^*	1.1			[11]
r_0	0.22			[27]
ϵ_b	7.5			[11]
Γ_j	$3.88/j^3$			[11,13]

V. CONCLUSIONS

In conclusion, we have developed a simple mathematical procedure to calculate, in the analytical form, the susceptibility of a superlattice with Rydberg excitons, taking, as an example, a Cu_2O/MgO SL, in the case of the normal incidence of the excited electromagnetic wave. With the help of the Kronig-Penney model for the superlattice, we have calculated effective masses of a hole and electron and then we have used the real density matrix approach to obtain resonances for any REs and the polariton dispersion relation. Periodic potentials of the SL structure cause the change of effective masses, which results in an increase of oscillator strengths and significantly shifts the positions of the excitonic resonances by over 1 eV. This sensitivity of the energy of excitonic resonances to the SL dimensions may provide an efficient way to measure mechanical deformation and temperature via thermal expansion of the lattice. The influence of the SL geometry, i.e., the well and barrier thicknesses, on the excitonic spectrum and the dispersion relation has been examined. It turned out that the periodic potential of the considered geometry leads to a significant anisotropy and either small or large value of the anisotropy factor α, which can be tuned depending on the intended structure application. Finally, we note that Rydberg excitons confined in a superlattice may be a promising platform for quantum computing technologies, being a solid-state analog of an atomic optical lattice, with a significant advantage of compactness and higher operating temperatures.

[1] C. Klingshirn, *Semiconductor Optics*, 2nd ed. (Springer, Berlin, 2005).

[2] D. Harankahage, J. Cassidy, M. Yang, D. Porotnikov, M. Williams, N. Kholmicheva, and M. Zamkov, Quantum computing with exciton qubits in colloidal semiconductor nanocrystals, J. Phys. Chem. C **125**, 22195 (2021).

[3] Y. Zhang, X. Zhang, B. Tang, C. Tian, C. Xu, H. Dong, and W. Zhou, Realization of an all-optically controlled dynamic superlattice for exciton-polaritons, Nanoscale **10**, 14082 (2018).

[4] S. Ghosh and T. C. H. Liew, Quantum computing with exciton-polariton condensates, npj Quantum Inf. **6**, 16 (2020).

[5] X. Zang, S. Montangero, L. D. Carr, and M. T. Lusk, Engineering and manipulating exciton wave packets, Phys. Rev. B **95**, 195423 (2017).

[6] M. J. Yang, P. V. Wadekar, W. C. Hsieh, H. C. Huang, C. W. Lin, J. W. Chou, C. H. Liao, C. F. Chang, H. W. Seo, S. T. You, L. W. Tu, I. K. Lo, N. J. Ho, S. W. Yeh, H. H. Liao, Q. Y. Chen, and W. K. Chu, MgO/Cu_2O Superlattices: growth of epitaxial

two-dimensional nanostructures, J. Electron. Mater. **45**, 6285 (2016).

[7] L. Isenhower, E. Urban, X. L. Zhang, A. T. Gill, T. Henage, T. A. Johnson, T. G. Walker, and M. Saffman, Demonstration of a neutral atom controlled-NOT quantum gate, Phys. Rev. Lett. **104**, 010503 (2010).

[8] A. Omran, H. Levine, A. Keesling, G. Semeghini, T. T. Wang, S. Ebadi, H. Bernien, A. S. Zibrov, H. Pichler, S. Choi, J. Cui, M. Rossignolo, P. Rembold, S. Montangero, T. Calarco, M. Endres, M. Greiner, V. Vuletic, and M. D. Lukin, Generation and manipulation of Schrödinger cat states in Rydberg atom arrays, Science **365**, 570 (2019).

[9] W. Li, A boost to Rydberg quantum computing, Nat. Phys. **16**, 820 (2020).

[10] A. V. Mazanik, A. I. Kulak, E. A. Bondarenko, O. V. Korolik, N. S. Mahon, and E. A. Streltso, Strong room temperature exciton photoluminescence in electrochemically deposited Cu_2O films, J. Lumin. **251**, 119227 (2022).

[11] T. Kazimierczuk, D. Fröhlich, S. Scheel, H. Stolz, and M. Bayer, Giant Rydberg excitons in the copper oxide Cu_2O, Nature (London) **514**, 343 (2014).

[12] M. A. M. Versteegh, S. Steinhauer, J. Bajo, T. Lettner, A. Soro, A. Romanova, S. Gyger, L. Schweickert, A. Mysyrowicz, and V. Zwiller, Giant Rydberg excitons in Cu_2O probed by photoluminescence excitation spectroscopy, Phys. Rev. B **104**, 245206 (2021).

[13] D. Ziemkiewicz and S. Zielińska-Raczyńska, Solid-state pulsed microwave emitter based on Rydberg excitons, Opt. Express **27**, 16983 (2019).

[14] M. Aßmann and M. Bayer, Semiconductor Rydberg physics, Adv. Quantum Technol. **3**, 1900134 (2020).

[15] C. Morin, J. Tignon J. Mangeney, S. Dhillon, G. Czajkowski, K. Karpiński, S. Zielińska-Raczyńska, D. Ziemkiewicz, and T. Boulier, Self-Kerr effect across the yellow Rydberg series of excitons in Cu_2O, Phys. Rev. Lett. **129**, 137401 (2022).

[16] S. Steinhauer, M. Versteegh, S. Gyger, A. Elshaari, B. Kunert, A. Mysyrowicz, and V. Zwiller, Rydberg excitons in Cu_2O microcrystals grown on a silicon platform, Commun. Mater. **1**, 11 (2020).

[17] M. Takahata, K. Tanaka, and N. Naka, Nonlocal optical response of weakly confined excitons in Cu_2O mesoscopic films, Phys. Rev. B **97**, 205305 (2018).

[18] J. DeLange, K. Barua, A. S. Paul, H. Ohadi, V. Zwiller, and S. Steinhauer, Highly-excited Rydberg excitons in synthetic thin-film cuprous oxide, Sci. Rep. **13**, 16881 (2023).

[19] V. Shahnazaryan, I. A. Shelykh, and O. Kyriienko, Attractive Coulomb interaction of 2D Rydberg excitons, Phys. Rev. B **93**, 245302 (2016).

[20] A. Konzelmann, B. Frank, and H. Giessen, Quantum confined Rydberg excitons in reduced dimensions, J. Phys. B: At. Mol. Opt. Phys. **53**, 024001 (2020).

[21] D. Ziemkiewicz, G. Czajkowski, K. Karpiński, and S. Zielińska-Raczyńska, Nonlinear optical properties and Kerr nonlinearity of Rydberg excitons in Cu_2O quantum wells, Phys. Rev. B **106**, 085431 (2022).

[22] K. Orfanakis, S. Rajendran, H. Ohadi, S. Zielińska-Raczyńska, G. Czajkowski, K. Karpiński, and D. Ziemkiewicz, Quantum confined Rydberg excitons in Cu_2O nanoparticles, Phys. Rev. B **103**, 245426 (2021).

[23] G. Bastard, *Wave Mechanics Applied to Semiconductor Heterostructures* (Les Editions de Physique, Paris, 1989).

[24] M. F. Pereira Jr., I. Galbraith, S. W. Koch, and G. Duggan, Exciton binding energies in semiconductor superlattices: An anisotropic-effective-medium approach, Phys. Rev. B **42**, 7084 (1990).

[25] G. Czajkowski, F. Bassani, and A. Tredicucci, Polaritonic effects in superlattices, Phys. Rev. B **54**, 2035 (1996).

[26] P. Schillak and G. Czajkowski, Optical properties of anisotropic II-VI superlattices, Phys. Status Solidi B **244**, 1627 (2007).

[27] S. Zielińska-Raczyńska, G. Czajkowski, and D. Ziemkiewicz, Optical properties of Rydberg excitons and polaritons, Phys. Rev. B **93**, 075206 (2016).

[28] D. Ziemkiewicz, K. Karpiński, G. Czajkowski, and S. Zielińska-Raczyńska, Excitons in Cu_2O: From quantum dots to bulk crystals and additional boundary conditions for Rydberg exciton-polaritons, Phys. Rev. B **101**, 205202 (2020).

[29] J. H. Davies, *The Physics of Low-dimensional Semiconductors, An Introduction* (Cambridge University Press, Cambridge, 1997).

[30] B. Balamurugan, I. Aruna, and B. R. Mehta, Size-dependent conductivity-type inversion in Cu_2O nanoparticles, Phys. Rev. B **69**, 165419 (2004).

[31] M. A. van Huis, A. van Veen, H. Schut, B. J. Kooi, and J. Th. M. De Hosson, Formation of solid Kr nanoclusters in MgO, Phys. Rev. B **67**, 235409 (2003).

[32] S. Siol, J. C. Hellmann, S. D. Tilley, M. Graetzel, J. Morasch, J. Deuermeier, W. Jaegermann, and A. Klein, Band alignment engineering at Cu_2O/ZnO heterointerfaces, ACS Appl. Mater. Interfaces **8**, 21824 (2016).

[33] I. S. Gradshteyn and I. M. Ryzhik, in *Table of Integrals, Series and Products*, 7th ed., edited by A. Jeffrey and D. Zwillinger (Academic Press, Amsterdam, 2007).

[34] M. Abramowitz and I. Stegun, *Handbook of Mathematical Functions* (Dover, New York, 1965).

[35] J. M. Luttinger and W. Kohn, Motion of electrons and holes in perturbed periodic fields, Phys. Rev. **97**, 869 (1955).

[36] H. Mathieu, P. Lefebvre, and Ph. Christol, Simple analytical method for calculating exciton binding energies in semiconductor quantum wells, Phys. Rev. B **46**, 4092 (1992).

[37] F. Bassani, G. Czajkowski, and A. Tredicucci, Polaritons in anisotropic semiconductors, Z. Phys. B **98**, 39 (1995).

[38] X. He, Fractional dimensionality and fractional derivative spectra of interband optical transitions, Phys. Rev. B **42**, 11751 (1990).

[39] S. Zielińska-Raczyńska, D. Ziemkiewicz, and G. Czajkowski, Magneto-optical properties of Rydberg excitons: Center-of-mass quantization approach, Phys. Rev. B **95**, 075204 (2017).

[40] K. Orfanakis, S. Rajendran, V. Walther, T. Volz, T. Pohl, and H. Ohadi, Rydberg exciton–polaritons in a Cu_2O microcavity, Nat. Mater. **21**, 767 (2022).

[41] D. P. Norton, Y. W. Heo, M. P. Ivill, K. Ip, S. J. Pearton, M. F. Chisholm, and T. Steiner, ZnO: Growth, doping and processing, Mater. Today **7**, 34 (2004).

[42] Q. Yan, P. Rinke, M. Winkelnkemper, A. Qteish, D. Bimberg, M. Scheffler, and C. G. Van de Walle, Strain effects and band parameters in MgO, ZnO, and CdO, Appl. Phys. Lett. **101**, 152105 (2012).

[43] N. Naka, I. Akimoto, M. Shirai, and K.-I. Kan'no, Time-resolved cyclotron resonance in cuprous oxide, Phys. Rev. B **85**, 035209 (2012).

[44] C. W. Miller, Z.-P. Li, I. K. Schuller, R. W. Dave, J. M. Slaughter, and J. Akerman, Dynamic spin-polarized resonant tunneling in magnetic tunnel junctions, Phys. Rev. Lett. **99**, 047206 (2007).

[45] H. Stolz, F. Schöne, and D. Semkat, Interaction of Rydberg excitons in cuprous oxide with phonons and photons: Optical linewidth and polariton effect, New J. Phys. **20**, 023019 (2018).

[46] J. Wang, Y. Tu, L. Yang, and H. Tolner, Theoretical investigation of the electronic structure and optical properties of zinc-doped magnesium oxide, J. Comput. Electron. **15**, 1521 (2016).